Attribution of the 2020 surge in atmospheric methane by inverse analysis of GOSAT observations

Zhen Qu[1], Daniel J. Jacob[1], Yuzhong Zhang[2], Lu Shen[3], Daniel J. Varon[1], Xiao Lu[4], Tia Scarpelli[1,5], Anthony Bloom[6], John Worden[6], Robert J. Parker[7,8]

[1] School of Engineering and Applied Science, Harvard University, Cambridge, MA, 02138, USA
[2] Key Laboratory of Coastal Environment and Resources of Zhejiang Province (KLaCER), School of Engineering, Westlake University, Hangzhou, Zhejiang, China
[3] Department of Atmospheric and Oceanic Sciences, School of Physics, Peking University, Beijing, China
[4] School of Atmospheric Sciences, Sun Yat-sen University, Zhuhai, Guangdong Province, China
[5] Department of Earth and Planetary Sciences, Harvard University, Cambridge, MA, 02138, USA
[6] Jet Propulsion Laboratory, California Institute of Technology, Pasadena, CA, USA
[7] National Centre for Earth Observation, University of Leicester, Leicester, UK
[8] Earth Observation Science, School of Physics and Astronomy, University of Leicester, UK

Abstract

Atmospheric methane mixing ratio rose by 15 ppbv between 2019 and 2020, the fastest growth rate on record. We conduct a global inverse analysis of 2019-2020 GOSAT satellite observations of atmospheric methane to analyze the combination of sources and sinks driving this surge. The atmospheric methane growth rate increased by 31 Tg a^{-1} from 2019 to 2020, representing a 36 Tg a^{-1} forcing on the methane budget away from steady state. 86% of the forcing in the base inversion is from increasing emissions (82 ± 18% in the 9-member inversion ensemble), and 14% is from decrease in tropospheric OH. Half of the increase in emissions is from Africa (15 Tg a^{-1}) and appears to be driven by wetland inundation. There is also a large relative increase in emissions from Canada and Alaska (4.8 Tg a^{-1}, 24%) that could be driven by temperature sensitivity of boreal wetland emissions.

1. Introduction

Methane (CH_4) is a potent greenhouse gas. Its atmospheric concentration has almost tripled since preindustrial time, resulting in a 1.2W m^{-2} radiative forcing and a 0.6°C increase in global mean surface air temperature [Szopa et al., 2021]. The concentration plateaued in 2000-2007 but has since resumed its increase with acceleration in recent years [Nisbet et al., 2019]. The annual rise in methane in 2020 was a record high of 15 ppbv, 50% larger than the 10 ppbv a^{-1} growth rate between 2015 and 2019 [Blunden and Boyer, 2021; NOAA, 2021a, b]. Here we use an inversion of GOSAT satellite observations of atmospheric methane to analyze the factors driving the 2020 surge.

Major anthropogenic sources of atmospheric methane include fossil fuels (oil, gas, and coal), livestock farming, rice cultivation, and waste management [Saunois et al., 2020]. Other sources

include wetlands, wildfires, and termites. Both wetlands and open fires have large interannual variability and may respond strongly to climate change [Ciais et al., 2013; Saunois et al., 2020]. Loss of methane is mainly by atmospheric oxidation by the hydroxyl radical (OH) in the troposphere, which is determined by complex chemistry and is also subject to interannual variability [Holmes et al., 2018]. COVID-19 shutdowns in 2020 were a major perturbation to economic activity but the effect on methane is unclear. Oil/gas production declined which would be expected to decrease methane emission in some regions [Lyon et al., 2021], but reduced maintenance of infrastructure could have caused increases [Laughner et al., 2021]. Decreases in emissions of nitrogen oxides ($NO_x \equiv NO + NO_2$) from fuel combustion led to decreases in free tropospheric ozone [Bouarar et al., 2021; Steinbrecht et al., 2021], which would decrease OH concentrations [Miyazaki et al., 2021] and hence the methane sink [Laughner et al., 2021].

Satellite observations of column-averaged dry methane mixing ratios (X_{CH4}) by solar backscatter in the shortwave infrared offer a unique resource to investigate the global changes in methane sources and sinks through inverse analysis [Jacob et al., 2016]. The Greenhouse Gases Observing Satellite (GOSAT) has been providing stable high-quality data since 2009 [Buchwitz et al., 2015; Kuze et al., 2009, 2016; Parker et al., 2020] and has been used extensively in inversions [Monteil et al., 2013; Cressot et al., 2014; Alexe et al., 2015; Pandey et al., 2016; Janardanan et al., 2020; Stanevich et al., 2021]. The recently launched TROPOspheric Monitoring Instrument (TROPOMI) provides a much higher data density of atmospheric methane [Hu et al., 2018; Lorente et al., 2021] but regional biases in the retrieval still limit its capability for global inversions [Qu et al., 2021]. In this work, we use the GOSAT X_{CH4} retrieval in a Bayesian analytical inversion to quantify the methane emissions and OH concentrations in 2019 and 2020, and their differences, in order to explain the 2020 surge.

2. Methods

2.1 Observations and model

We use the University of Leicester version 9.0 GOSAT methane retrieval [Parker and Boesch, 2020]. This product has a good consistency (3.9 ppbv regional bias) with ground-based methane column measurements from TCCON [Parker et al., 2020] and good consistency with surface data in estimating global methane sources through inversions [Lu et al., 2021, 2022]. We use observations over both land and ocean, the latter in glint mode [Parker et al., 2020]. We only include high-quality retrievals with "xch4_quality_flag" = 0.

We use the GEOS-Chem chemical transport model version 12.5.0 (10.5281/zenodo.3403111) at 2°×2.5° grid resolution to relate methane emissions to X_{CH4} as retrieved by GOSAT. Model transport is driven by NASA MERRA-2 archived meteorological fields. The model is essentially linear except for a small nonlinearity from the optimization of OH concentrations [Maasakkers et al., 2019]. We use the same prior emission estimates for 2019 and 2020 in the simulations, including the Global Fuel Exploitation Inventory (GFEI) version 2.0 [Scarpelli et al., 2022] for oil, gas, and coal exploitation; the EDGAR v4.3.2 inventory [Janssens-Maenhout et al., 2019] for other anthropogenic sources; and monthly mean 2019 wetland emissions from the nine highest-performance members of the WetCHARTs v1.3.2 inventory ensemble [Ma et al., 2021]. Loss of methane from oxidation by tropospheric OH is calculated with archived 3-D climatological

monthly fields of OH concentrations from a GEOS-Chem full-chemistry simulation [Wecht et al., 2014], with a corresponding methane lifetime of 10.5 years. Other minor sinks from oxidation by tropospheric Cl and in the stratosphere, and from uptake by soils, are the same as in Qu et al. [2021]. Initial model concentrations of methane on January 1, 2019 and January 1, 2020 are adjusted by a global scaling factor of 0.97 and 1.01 to match GOSAT X_{CH4}.

2.2 Inverse analysis

We perform two independent Bayesian analytical inversions to estimate the sources and sinks of methane for 2019 and 2020. The inversion draws on GOSAT observations $\boldsymbol{y}$ together with the above prior estimates for emissions and OH concentrations. The differences in 2019 and 2020 inversion results are solely driven by observations. For each year, the inversion optimizes a state vector $\boldsymbol{x}$ consisting of (1) annual mean non-wetland methane emissions for land-containing 2°×2.5° grid cells (4020 elements), (2) monthly wetland methane emissions for 14 subcontinental regions (168 elements), and (3) annual hemispheric methane loss frequency against oxidation by tropospheric OH (2 elements for the Northern and Southern hemisphere). Previous work has shown that inversion of GOSAT observations can provide independent information on global emissions and OH concentrations as indicated by inspection of the posterior error correlation matrix [Maasakkers et al., 2019; Y. Zhang et al., 2021].

For each year, we perturb each of the state vector elements in 4190 GEOS-Chem simulations to construct the full Jacobian matrix $\mathbf{K}$. Since the relationship between $\boldsymbol{x}$ and $\boldsymbol{y}$ is approximately linear, $\mathbf{K}$ describes the sensitivity of the methane observations to the state vector as simulated by GEOS-Chem. The posterior estimate with Gaussian error statistics is obtained by minimizing the scalar cost function $J(\boldsymbol{x})$:

$$J(\boldsymbol{x}) = (\boldsymbol{x} - \boldsymbol{x_a})^T \mathbf{S_a}^{-1} (\boldsymbol{x} - \boldsymbol{x_a}) + \gamma (\boldsymbol{y} - \mathbf{K}\boldsymbol{x})^T \mathbf{S_o}^{-1} (\boldsymbol{y} - \mathbf{K}\boldsymbol{x}), \quad (1)$$

where $\boldsymbol{x_a}$ is the prior estimate of the state vector, $\mathbf{S_a}$ is the prior error covariance matrix, $\mathbf{S_o}$ is the observational error covariance matrix assumed to be diagonal, and γ is a regularization parameter that accounts for the effect of unresolved correlation in the observational error. $\mathbf{S_a}$ is constructed with a 10% error for annual mean OH concentrations and a 50% error for all emissions. Prior error correlations for monthly wetland emissions in the 14 subcontinental regions are calculated using the WetCHARTs model ensemble [Bloom et al., 2017; Y. Zhang et al., 2021]. Diagonal elements of $\mathbf{S_o}$ are calculated using the residual error method [Heald et al., 2004], resulting in a mean observational error standard deviation of 14 ppb. γ is chosen to be 0.5 based on the L-curve test (Figure S1).

The best posterior estimate of $\boldsymbol{x}$ is given by [Rodgers, 2000]:

$$\hat{\boldsymbol{x}} = \boldsymbol{x_a} + \left(\gamma \mathbf{K}^T \mathbf{S_o}^{-1} \mathbf{K} + \mathbf{S_a}^{-1}\right)^{-1} \gamma \mathbf{K}^T \mathbf{S_O}^{-1} (\boldsymbol{y} - \mathbf{K}\boldsymbol{x_a}). \quad (2)$$

with posterior error covariance matrix $\hat{\mathbf{S}}$:

$$\hat{\mathbf{S}} = (\gamma \mathbf{K}^T \mathbf{S_o}^{-1} \mathbf{K} + \mathbf{S_a}^{-1})^{-1}. \quad (3)$$

The posterior solution can also be presented in reduced aggregated form for emission sectors and regions with a matrix **W** to represent the linear transformation from the full state vector to the reduced state vector. We do this in particular to estimate errors and error correlations in inversion results for the global and continental differences in the methane budget between 2019 and 2020. The posterior estimate of the reduced state vector ($\hat{\boldsymbol{x}}_{\boldsymbol{red}}$) is computed as

$$\hat{\boldsymbol{x}}_{\boldsymbol{red}} = \mathbf{W}\hat{\boldsymbol{x}}. \quad (4)$$

and its posterior error covariance is given by

$$\hat{\mathbf{S}}_{\boldsymbol{red}} = \mathbf{W}\hat{\mathbf{S}}\mathbf{W}^{\mathbf{T}}. \quad (5)$$

The posterior error covariance matrix estimates error statistics under the assumption that the prior error covariance assumptions are correct, but there is uncertainty in these parameters. The assumption that prior errors on anthropogenic emissions are spatially uncorrelated can lead to an underestimate of posterior errors when aggregating emissions. As a complementary approach to estimate errors, we conducted an inversion ensemble with varying parameters from our base inversion one at a time, including prior error standard deviations for anthropogenic emissions (30% and 60%), wetland emissions (20% and 60%), and OH concentrations (5% and 20%), and different regularization parameters ($\gamma = 0.1$ and 1). This results in a 9-member inversion ensemble including the base inversion. This ensemble provides insight on the role of uncertainty assumptions on the attribution of 2019-2020 methane changes, and we take the mean and standard deviation of the optimized results for that ensemble as a better estimate of the error on our posterior estimates.

3. Results

Figure 1 shows the global distribution of GOSAT annual mean X_{CH4} differences between 2019 and 2020. The global averaged GOSAT methane increased by 13.4 ppbv from 2019 to 2020. Continental regions increased more than the oceans, arguing against a dominant role of the methane sink in driving the 2020 surge (methane sources are continental, while the sink from oxidation is distributed across ocean and land). Some continental regions show particularly large increases including Central Africa, Europe, northern Brazil, and North America. China, the largest anthropogenic methane source [Janssens-Maenhout et al., 2019], shows weaker increases. However, such year-to-year comparisons in methane concentrations may have sampling bias and not necessarily relate to changes in emissions because atmospheric transport also drives interannual variability [Bruhwiler et al., 2017; Feng et al., 2021]. The inversion allows us to correct for the effect of transport and isolate the contributions from changes in sources and sinks.

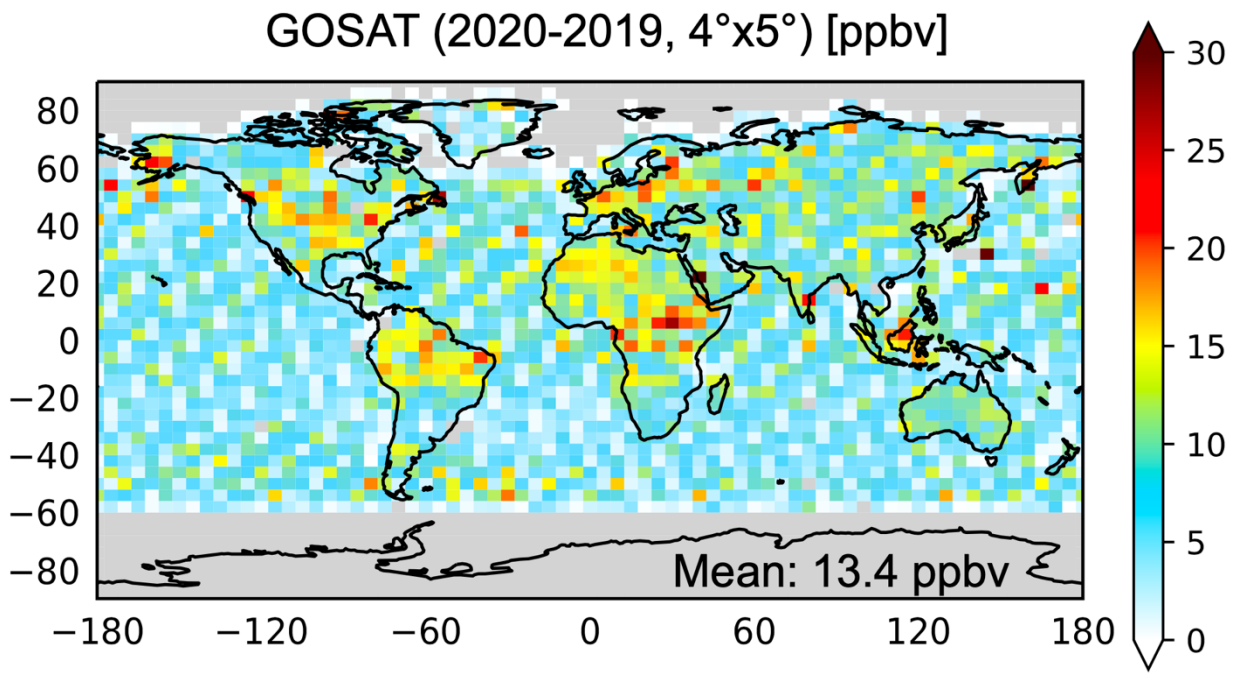

Figure 1. Methane changes from 2019 to 2020 measured by the GOSAT satellite instrument as the difference in annual mean dry column mixing ratio (X_{CH4}) mapped on a 4°×5° grid. The global mean increase is 13.4 ppb. 5% of the 4°×5° grid cells show decreases from 2019 to 2020. Areas in grey do not have observations in either 2019 or 2020.

Table 1 summarizes our inversion results. GEOS-Chem simulations using posterior emission and OH estimates show a 42 Tg increase (0.8%) in the atmospheric mass of methane from 2019 to 2020, corresponding to a 13.7 ppbv increase in X_{CH4} as would be sampled by GOSAT. Methane emissions increase by 31 Tg a^{-1} from 2019 to 2020 in the base inversion while the sink from oxidation by tropospheric OH decreases by 1.0 Tg a^{-1}. $\hat{\mathbf{S}}_{red}$ (Equation 5) shows that 2019-2020 changes in methane sources and sinks have a strong error correlation (r=0.97) but that the posterior errors are small, with 90% confidence that the increase of methane emission is in the range of 25 – 37 Tg a^{-1} and that the change in the methane sink due to changes in OH is in the range of -6 – 4 Tg a^{-1}. As pointed out above, this could underestimate the actual uncertainty in the solution. Analysis of the inversion ensemble as individual realizations of the solution, shown in Table 1 and Table S1, confirms the dominance of increase in methane emissions (mean ± standard deviation: 30 ± 5.5 Tg a^{-1}) as a principal driver for the 2019-2020 rise in methane concentrations, while finding that the change in the methane sink is a minor contributor (- 2.6 ± 6.7 Tg a^{-1}).

The results from the inversion can be interpreted with a simple mass balance analysis. The global growth rate of tropospheric methane mass dm/dt is determined by a balance between methane emission E, oxidation by tropospheric OH (loss frequency k), and other minor losses L not optimized in the inversion:

$$\frac{dm}{dt} = E - km \quad - L, \qquad (6)$$

The change in imbalance or acceleration of methane growth (d^2m/dt^2) between 2019 and 2020 can be expressed as:

$$\frac{d^2m}{dt^2} = \frac{dE}{dt} - k\frac{dm}{dt} - m\frac{dk}{dt} - \frac{dL}{dt}, \quad (7)$$

where $dE/dt = E_{2020} - E_{2019}$ is the change in methane emissions, $dm/dt = m_{2020} - m_{2019}$ is the change in methane mass, $dk/dt = k_{2020} - k_{2019}$ is the change driven by OH, and $dL/dt = L_{2020} - L_{2019}$ is the change due to other minor sinks. We define the forcing F on the methane budget as:

$$F = \frac{dE}{dt} - m\frac{dk}{dt}, \quad (8)$$

which describes the total changes in methane emissions and OH concentrations that force the methane concentration away from first-order relaxation to steady state. F can be largely derived from observations since it is given equivalently by $F = d^2m/dt^2 + kdm/dt + dL/dt$.

The base inversion results as given in Table 1 show a 5.4% increase in global methane emissions (dE/dt) from 2019 to 2020, a 1.2% decrease in area-weighted global mean tropospheric OH concentrations. The decrease in OH drives a 5 Tg a^{-1} (mdk/dt) forcing of the methane budget to offset the increase in methane mass, which for constant OH causes an increase in the sink of 4 Tg a^{-1} (kdm/dt). The dL/dt term for other methane losses is small (1 Tg a^{-1}) and is in the model solely determined by increase in methane mass (no forcing). The forcing on the methane budget from 2019 to 2020 is thus 36 Tg a^{-1}, of which 31 Tg a^{-1} (86%) is from emissions and 5 Tg a^{-1} (14%) is from the decrease in tropospheric OH in our base inversion. For our 9-member inversion ensemble, the contribution to the 36 Tg a^{-1} forcing from emissions is 30 ± 5.5 Tg a^{-1} (82 ± 18%), with OH contributing the remainder.

The 1.2% OH decrease from 2019 to 2020 in our base inversion (1.6 ± 1.5% in the 9-member inversion ensemble) is lower than the 2-4% decrease inferred by Miyazaki et al. [2021] for the first half of 2020 based on chemical data assimilation of satellite observations and attributed to NO_x emission decreases from COVID-19 lockdowns. These lockdowns relaxed in the second half of 2020 and OH could have recovered. Laughner et al. [2021] found in a box model analysis that a 3% reduction in global mean OH concentration in 2020 could account for only half of the observed methane increase, which is consistent with our results that OH changes cannot explain most of the 2020 methane surge.

Table 1. Global 2019-2020 methane budget from inverse analysis of GOSAT data.

	2019	2020	2020-2019[a]
Atmospheric mass [Tg]	5197	5238	41 (42 ± 0.67)
Total Sources [Tg a^{-1}]	572	603	31 (30 ± 5.5)
Total Sinks [Tg a^{-1}]	544	544	-0.2 (-1.8 ± 6.7)
Tropospheric OH	469	468	-1.0 (-2.6 ± 6.7)
Others [b]	75	76	0.8

Growth rate [Tg a^{-1}][c]	**28**	**59**	**31** (31 ± 1.2)
Lifetime (OH) [a] [d]	11.06	11.21	0.15 (0.20 ± 0.17)

[a] Values from the base inversion, with means and standard deviations from the 9-member inversion ensemble in parentheses.
[b] Including oxidation in the stratosphere and by tropospheric Cl, and uptake by soils. These minor sinks are not optimized in the inversion and their small increase from 2019 to 2020 (same for all inversion ensemble members) is due solely to the increase in methane mass driving an increase in the oxidation loss rate.
[c] Growth rate in atmospheric methane as determined by the imbalance between sources and sinks.
[d] Lifetime of total atmospheric methane against oxidation by tropospheric OH.

We went on to further analyze the GOSAT inversion results in terms of the sources contributing to the global 2019-2020 change in methane emissions. We find that we cannot robustly separate the contributions from anthropogenic and wetland emissions, or from different anthropogenic sectors, as indicated by error correlations and the spread of results in the inversion ensemble. However, we can separate the contributions from individual continental regions. Figure 2 and Table 2 show those results. $\hat{\mathbf{S}}_{red}$ for the base inversion finds only moderate error correlation between different regions (Figure 2a) and the inversion ensemble also indicates consistent results for the major regions driving the change (Table 2).

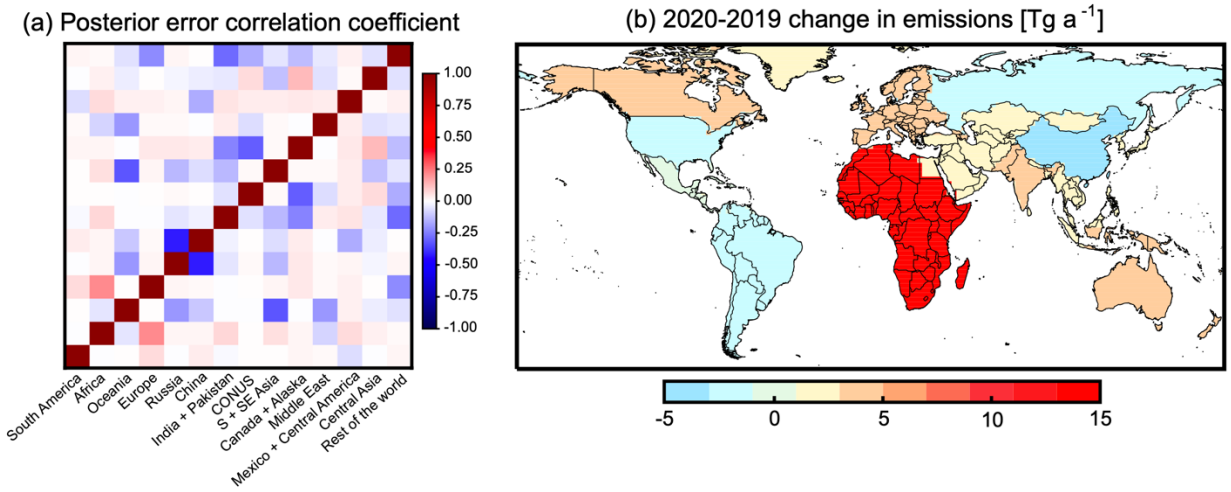

Figure 2. Change in methane emissions from 2019 to 2020 for large continental regions as given by the base inversion of GOSAT observations. The left panel shows the posterior error correlations for the emission changes between regions. Ranges from the inversion ensemble are given in Table 2.

Figure 2 (b) shows that Africa accounts for 48% of the global increase in methane emissions from 2019 to 2020 with the rest spread across other continental regions and some regions (China, CONUS, South America, Russia) showing a decrease. These results are consistent across the inversion ensemble (Table 2). Africa shows an increase of 15 Tg a^{-1} in methane emissions from 2019 to 2020. We attribute most of the increase to wetland emissions in East Africa (30°E-50°E, 15°S-10°N) due to the increases in rainfall by 20% (46 mm) in the first three seasons from 2019 to 2020 according to TAMSAT (http://www.tamsat.org.uk/index.php/data). Consistent with the

increase in rainfall, the water flows of the Congo-Oubangui River, which goes through wetlands in the Congo Basin, were much higher in 2020 than in previous years [World Meteorological Organization, 2022]. Flooding in 2020 was widespread, affecting 50% more East Africans than in 2019 [BBC, 2020]. Wetland methane emission in the tropics is dominantly controlled by water table depth, and interannual variability is primarily driven by precipitation and inundation [Bloom et al., 2010; Lunt et al., 2019]. The rapid increase in livestock emissions in East Africa [Y. Zhang et al., 2021] could also contribute to the surge. The large relative increase of methane emissions in Canada and Alaska (4.8 Tg a^{-1} or 24%) can be attributed to a temperature-driven increase in wetland emissions as shown by WetCHARTs (Figure S2). The decrease in China could reflect the continued decline of emissions from coal mines [Y. Zhang et al., 2021] and rice [G. Zhang et al., 2020]. The decrease in CONUS could reflect the continued decline of emissions from the oil/gas sector [Lu et al., 2022].

Table 2. Regional methane emissions and 2020-2019 differences[a]

	Prior	2019	2020	2020 – 2019	
	[Tg a^{-1}]	[Tg a^{-1}]	[Tg a^{-1}]	[Tg a^{-1}]	[%]
South America	92	120	117	-2.7 (-2.8 ± 0.98)	-2.3 (-2.4 ± 0.87)
Africa	81	80	95	15 (14 ± 1.6)	18 (18 ± 1.9)
Oceania	26	32	35	3.2 (2.7 ± 1.7)	10 (8.6 ± 5.4)
Europe	34	32	37	4.6 (4.4 ± 0.68)	14 (14 ± 2.1)
Russia	32	39	38	-1.1 (-1.1 ± 0.39)	-2.9 (-2.7 ± 1.0)
China	64	51	47	-3.9 (-3.7 ± 0.47)	-7.8 (-7.3 ± 1.0)
India + Pakistan	38	47	50	3.5 (3.5 ± 0.53)	7.4 (7.4 ± 1.1)
CONUS	34	44	42	-2.0 (-1.8 ± 0.29)	-4.6 (-4.2 ± 0.57)
S + SE Asia	22	29	31	2.0 (1.9 ± 0.40)	6.7 (6.5 ± 1.3)
Canada + Alaska	19	20	25	4.8 (4.9 ± 0.16)	24 (24 ± 0.81)
Middle East	17	21	24	2.5 (2.5 ± 0.13)	12 (12 ± 0.64)
Mexico + Central America	14	19	19	-0.49 (-0.54 ± 0.34)	-2.6 (-2.8 ± 1.8)
Central Asia	11	16	18	2.5 (2.3 ± 0.35)	16 (15 ± 1.9)
Rest of the world	23	24	25	1.7 (1.4 ± 1.1)	7.3 (6.0 ± 4.5)

[a] Values from the base inversion, with means and standard deviations from the 9-member inversion ensemble in parentheses. Prior and posterior emissions include both anthropogenic and natural sources.

4. Conclusions

We conducted a global inverse analysis of 2019-2020 GOSAT observations to analyze the factors driving the 2020 surge in atmospheric methane concentrations. The inversion shows an increase in the methane growth rate from 28 Tg a^{-1} in 2019 to 59 Tg a^{-1} in 2020, consistent with observations. This implies a forcing on the methane budget away from a steady state by 36 Tg a^{-1} from 2019 to 2020, 86% (82 ± 18% in the 9-member inversion ensemble) of which is from the increase in emissions between the two years and the rest is from the decrease in tropospheric OH. The global

mean OH concentration decreases by 1.2% (1.6 ± 1.5%) from 2019 to 2020, which could be due to reduced NO_x emissions from COVID-19 decreases in economic activity but accounts for only a small fraction of the methane surge. We find that half of the increase in methane emissions from 2019 to 2020 is due to Africa. High precipitation and flooding in East Africa leading to increased wetland methane emissions could explain the increase. We also find a large relative increase in Canadian emissions, also apparently driven by wetlands. Our finding of wetlands as the principal driver for the 2020 surge could be a harbinger for the response of atmospheric methane to climate change.

Acknowledgments

This work was funded by the NASA Carbon Monitoring System under NASA award number 80NSSC18K0178 to Harvard University. RJP is funded via the UK National Centre for Earth Observation (NE/N018079/1). We thank the Japanese Aerospace Exploration Agency, National Institute for Environmental Studies, and the Ministry of Environment for the GOSAT data and their continuous support as part of the Joint Research Agreement. This research used the ALICE High Performance Computing Facility at the University of Leicester for the GOSAT retrievals.

Data availability statement

The GOSAT methane retrieval is available at https://www.leos.le.ac.uk/data/GHG/GOSAT/v9.0/CH4_GOS_OCPR_v9.0_final_nceo_2009_2020.tar.gz (last accessed May 3, 2022).

References

Alexe, M., Bergamaschi, P., Segers, A., Detmers, R., Butz, A., Hasekamp, O., et al. (2015). Inverse modelling of CH_4 emissions for 2010–2011 using different satellite retrieval products from GOSAT and SCIAMACHY. *Atmos. Chem. Phys., 15*(1), 113-133. https://acp.copernicus.org/articles/15/113/2015/

BBC, Flooding hits six million people in East Africa, available at: https://www.bbc.com/news/world-africa-54433904, 2020.

Bouarar, I., Gaubert, B., Brasseur, G. P., Steinbrecht, W., Doumbia, T., Tilmes, S., et al. (2021). Ozone Anomalies in the Free Troposphere During the COVID-19 Pandemic. *Geophysical Research Letters, 48*(16), e2021GL094204. https://agupubs.onlinelibrary.wiley.com/doi/abs/10.1029/2021GL094204

Bloom, A. A., Palmer, P. I., Fraser, A., Reay, D. S., & Frankenberg, C. (2010). Large-Scale Controls of Methanogenesis Inferred from Methane and Gravity Spaceborne Data. *Science, 327*(5963), 322-325. https://www.science.org/doi/abs/10.1126/science.1175176.

Bloom, A. A., Bowman, K. W., Lee, M., Turner, A. J., Schroeder, R., Worden, J. R., et al. (2017). A global wetland methane emissions and uncertainty dataset for atmospheric chemical transport models (WetCHARTs version 1.0). *Geosci. Model Dev., 10*(6), 2141-2156. https://gmd.copernicus.org/articles/10/2141/2017/

Blunden, J. and T. Boyer, Eds., 2020: "State of the Climate in 2020". Bull. Amer. Meteor. Soc., 102 (8), Si–S475, doi:10.1175/2021BAMSStateoftheClimate.1.

Bruhwiler, L. M., Basu, S., Bergamaschi, P., Bousquet, P., Dlugokencky, E., Houweling, S., et al. (2017). U.S. CH4 emissions from oil and gas production: Have recent large increases been detected? *Journal of Geophysical Research: Atmospheres, 122*(7), 4070-4083. https://agupubs.onlinelibrary.wiley.com/doi/abs/10.1002/2016JD026157

Buchwitz, M., Reuter, M., Schneising, O., Boesch, H., Guerlet, S., Dils, B., et al. (2015). The Greenhouse Gas Climate Change Initiative (GHG-CCI): Comparison and quality assessment of near-surface-sensitive satellite-derived CO2 and CH4 global data sets. *Remote Sensing of Environment, 162*, 344-362. http://www.sciencedirect.com/science/article/pii/S0034425713003520

Ciais, P., Sabine, C., Bala, G., Bopp, L., Brovkin, V., Canadell, J., Chhabra, A., DeFries, R., Galloway, J., Heimann, M., Jones, C., Le Quéré, C., Myneni, R. B., Piao, S., and Thornton, P.: Carbon and Other Biogeochemical Cycles, in: Climate Change 2013: The Physical Science Basis. Contribution of Working Group I to the Fifth Assessment Report of the Intergovernmental Panel on Climate Change, edited by: Stocker, T. F., Qin, D., Plattner, G.-K., Tignor, M., Allen, S. K., Boschung, J., Nauels, A., Xia, Y., Bex, V., and

Midgley, P. M., Cambridge University Press, Cambridge, United Kingdom and New York, NY, USA, 1535 pp., 2013

Cressot, C., Chevallier, F., Bousquet, P., Crevoisier, C., Dlugokencky, E. J., Fortems-Cheiney, A., et al. (2014). On the consistency between global and regional methane emissions inferred from SCIAMACHY, TANSO-FTS, IASI and surface measurements. *Atmos. Chem. Phys., 14*(2), 577-592. https://acp.copernicus.org/articles/14/577/2014/

Feng L., S. Tavakkoli, S. Jordaan, A. Andrews, J. S. Benmergui, and S. M. Miller, Ambiguity in recent changes to US methane emissions, AGU Fall Meeting, 2021.

Heald, C. L., Jacob, D. J., Jones, D. B. A., Palmer, P. I., Logan, J. A., Streets, D. G., et al. (2004). Comparative inverse analysis of satellite (MOPITT) and aircraft (TRACE-P) observations to estimate Asian sources of carbon monoxide. *Journal of Geophysical Research: Atmospheres, 109*(D23). https://agupubs.onlinelibrary.wiley.com/doi/abs/10.1029/2004JD005185

Hu, H., Landgraf, J., Detmers, R., Borsdorff, T., Aan de Brugh, J., Aben, I., et al. (2018). Toward Global Mapping of Methane With TROPOMI: First Results and Intersatellite Comparison to GOSAT. *Geophys. Res. Lett., 45*(8), 3682-3689. https://agupubs.onlinelibrary.wiley.com/doi/abs/10.1002/2018GL077259

Jacob, D. J., Turner, A. J., Maasakkers, J. D., Sheng, J., Sun, K., Liu, X., et al. (2016). Satellite observations of atmospheric methane and their value for quantifying methane emissions. *Atmos. Chem. Phys., 16*(22), 14371-14396. https://acp.copernicus.org/articles/16/14371/2016/

Janssens-Maenhout, G., Crippa, M., Guizzardi, D., Muntean, M., Schaaf, E., Dentener, F., et al. (2019). EDGAR v4.3.2 Global Atlas of the three major greenhouse gas emissions for the period 1970–2012. *Earth Syst. Sci. Data, 11*(3), 959-1002. https://essd.copernicus.org/articles/11/959/2019/

Janardanan, R., Maksyutov, S., Tsuruta, A., Wang, F., Tiwari, Y. K., Valsala, V., et al. (2020). Country-Scale Analysis of Methane Emissions with a High-Resolution Inverse Model Using GOSAT and Surface Observations. *Remote Sensing, 12*(3), 375. https://www.mdpi.com/2072-4292/12/3/375

Kuze, A., Suto, H., Nakajima, M., & Hamazaki, T. (2009). Thermal and near infrared sensor for carbon observation Fourier-transform spectrometer on the Greenhouse Gases Observing Satellite for greenhouse gases monitoring. *Applied Optics, 48*(35), 6716-6733. http://opg.optica.org/ao/abstract.cfm?URI=ao-48-35-6716

Kuze, A., Suto, H., Shiomi, K., Kawakami, S., Tanaka, M., Ueda, Y., et al. (2016). Update on GOSAT TANSO-FTS performance, operations, and data products after more than 6 years

in space. *Atmos. Meas. Tech., 9*(6), 2445-2461. https://amt.copernicus.org/articles/9/2445/2016/

Laughner, J. L., Neu, J. L., Schimel, D., Wennberg, P. O., Barsanti, K., Bowman, K. W., et al. (2021). Societal shifts due to COVID-19 reveal large-scale complexities and feedbacks between atmospheric chemistry and climate change. *Proceedings of the National Academy of Sciences, 118*(46), e2109481118. https://www.pnas.org/doi/abs/10.1073/pnas.2109481118.

Lu, X., Jacob, D. J., Zhang, Y., Maasakkers, J. D., Sulprizio, M. P., Shen, L., et al. (2021). Global methane budget and trend, 2010–2017: complementarity of inverse analyses using in situ (GLOBALVIEWplus CH4 ObsPack) and satellite (GOSAT) observations. *Atmos. Chem. Phys., 21*(6), 4637-4657. https://acp.copernicus.org/articles/21/4637/2021/

Lunt, M. F., Palmer, P. I., Feng, L., Taylor, C. M., Boesch, H., & Parker, R. J. (2019). An increase in methane emissions from tropical Africa between 2010 and 2016 inferred from satellite data. *Atmos. Chem. Phys., 19*(23), 14721-14740. https://acp.copernicus.org/articles/19/14721/2019/

Lyon, D. R., Hmiel, B., Gautam, R., Omara, M., Roberts, K. A., Barkley, Z. R., et al. (2021). Concurrent variation in oil and gas methane emissions and oil price during the COVID-19 pandemic. *Atmos. Chem. Phys., 21*(9), 6605-6626. https://acp.copernicus.org/articles/21/6605/2021/

Lorente, A., Borsdorff, T., Butz, A., Hasekamp, O., aan de Brugh, J., Schneider, A., et al. (2021). Methane retrieved from TROPOMI: improvement of the data product and validation of the first 2 years of measurements. *Atmos. Meas. Tech., 14*(1), 665-684. https://amt.copernicus.org/articles/14/665/2021/

Lu, X., Jacob, D. J., Wang, H., Maasakkers, J. D., Zhang, Y., Scarpelli, T. R., et al. (2022). Methane emissions in the United States, Canada, and Mexico: evaluation of national methane emission inventories and 2010–2017 sectoral trends by inverse analysis of in situ (GLOBALVIEWplus CH4 ObsPack) and satellite (GOSAT) atmospheric observations. *Atmos. Chem. Phys., 22*(1), 395-418. https://acp.copernicus.org/articles/22/395/2022/

Ma, S., Worden, J. R., Bloom, A. A., Zhang, Y., Poulter, B., Cusworth, D. H., et al. (2021). Satellite Constraints on the Latitudinal Distribution and Temperature Sensitivity of Wetland Methane Emissions. *AGU Advances, 2*(3), e2021AV000408. https://agupubs.onlinelibrary.wiley.com/doi/abs/10.1029/2021AV000408

Maasakkers, J. D., Jacob, D. J., Sulprizio, M. P., Scarpelli, T. R., Nesser, H., Sheng, J. X., et al. (2019). Global distribution of methane emissions, emission trends, and OH concentrations and trends inferred from an inversion of GOSAT satellite data for 2010–2015. *Atmos. Chem. Phys., 19*(11), 7859-7881. https://acp.copernicus.org/articles/19/7859/2019/

Miyazaki, K., Bowman, K., Sekiya, T., Takigawa, M., Neu, J. L., Sudo, K., et al. (2021). Global tropospheric ozone responses to reduced NO_x emissions linked to the COVID-19 worldwide lockdowns. *Science Advances, 7*(24), eabf7460. https://www.science.org/doi/abs/10.1126/sciadv.abf7460.

Monteil, G., Houweling, S., Butz, A., Guerlet, S., Schepers, D., Hasekamp, O., et al. (2013). Comparison of CH4 inversions based on 15 months of GOSAT and SCIAMACHY observations. *Journal of Geophysical Research: Atmospheres, 118*(20), 11,807-811,823. https://agupubs.onlinelibrary.wiley.com/doi/abs/10.1002/2013JD019760

Nisbet, E. G., Manning, M. R., Dlugokencky, E. J., Fisher, R. E., Lowry, D., Michel, S. E., et al. (2019). Very Strong Atmospheric Methane Growth in the 4 Years 2014–2017: Implications for the Paris Agreement. *Global Biogeochemical Cycles, 33*(3), 318-342. https://agupubs.onlinelibrary.wiley.com/doi/abs/10.1029/2018GB006009

NOAA (2021a), The NOAA Annual Greenhous Gas Index, available at https://gml.noaa.gov/aggi/aggi.html.

NOAA (2021b), Despite pandemic shutdowns, carbon dioxide and methane surged in 2020, available at https://research.noaa.gov/article/ArtMID/587/ArticleID/2742/Despite-pandemic-shutdowns-carbon-dioxide-and-methane-surged-in-2020.

Pandey, S., Houweling, S., Krol, M., Aben, I., Chevallier, F., Dlugokencky, E. J., et al. (2016). Inverse modeling of GOSAT-retrieved ratios of total column CH4 and CO2 for 2009 and 2010. *Atmos. Chem. Phys., 16*(8), 5043-5062. https://acp.copernicus.org/articles/16/5043/2016/

Parker, R. J., Webb, A., Boesch, H., Somkuti, P., Barrio Guillo, R., Di Noia, A., et al. (2020). A Decade of GOSAT Proxy Satellite CH4 Observations. *Earth Syst. Sci. Data Discuss., 2020*, 1-36. https://essd.copernicus.org/preprints/essd-2020-114/

Parker, R. J. and Boesch, H. (2020). University of Leicester GOSAT Proxy XCH4 v9.0, Centre for Environmental Data Analysis, 7 May 2020, https://doi.org/10.5285/18ef8247f52a4cb6a14013f8235cc1eb.

Qu, Z., Jacob, D. J., Shen, L., Lu, X., Zhang, Y., Scarpelli, T. R., et al. (2021). Global distribution of methane emissions: a comparative inverse analysis of observations from the TROPOMI and GOSAT satellite instruments. *Atmos. Chem. Phys., 21*(18), 14159-14175. https://acp.copernicus.org/articles/21/14159/2021/

Rodgers, C. D.: Inverse Methods for Atmospheric Sounding: Theory and Practice, World Scientific, River Edge, USA, 2000.

Saunois, M., Stavert, A. R., Poulter, B., Bousquet, P., Canadell, J. G., Jackson, R. B., et al. (2020). The Global Methane Budget 2000–2017. *Earth Syst. Sci. Data, 12*(3), 1561-1623. https://essd.copernicus.org/articles/12/1561/2020/

Scarpelli, T. R., Jacob, D. J., Grossman, S., Lu, X., Qu, Z., Sulprizio, M. P., et al. (2022). Updated Global Fuel Exploitation Inventory (GFEI) for methane emissions from the oil, gas, and coal sectors: evaluation with inversions of atmospheric methane observations. *Atmos. Chem. Phys., 22*(5), 3235-3249. https://acp.copernicus.org/articles/22/3235/2022/

Stanevich, I., Jones, D. B. A., Strong, K., Keller, M., Henze, D. K., Parker, R. J., et al. (2021). Characterizing model errors in chemical transport modeling of methane: using GOSAT XCH4 data with weak-constraint four-dimensional variational data assimilation. *Atmos. Chem. Phys., 21*(12), 9545-9572. https://acp.copernicus.org/articles/21/9545/2021/

Steinbrecht, W., Kubistin, D., Plass-Dülmer, C., Davies, J., Tarasick, D. W., von der Gathen, P., et al. (2021). COVID-19 Crisis Reduces Free Tropospheric Ozone Across the Northern Hemisphere. *Geophysical Research Letters, 48*(5), e2020GL091987. https://agupubs.onlinelibrary.wiley.com/doi/abs/10.1029/2020GL091987

Szopa, S., V. Naik, B. Adhikary, P. Artaxo, T. Berntsen, W.D. Collins, S. Fuzzi, L. Gallardo, A. Kiendler Scharr, Z. Klimont, H. Liao, N. Unger, and P. Zanis (2021). Short-Lived Climate Forcers. In Climate Change 2021: The Physical Science Basis. Contribution of Working Group I to the Sixth Assessment Report of the Intergovernmental Panel on Climate Change [Masson-Delmotte, V., P. Zhai, A. Pirani, S.L. Connors, C. Péan, S. Berger, N. Caud, Y. Chen, L. Goldfarb, M.I. Gomis, M. Huang, K. Leitzell, E. Lonnoy, J.B.R. Matthews, T.K. Maycock, T. Waterfield, O. Yelekçi, R. Yu, and B. Zhou (eds.)]. Cambridge University Press. In Press.

Wecht, K. J., Jacob, D. J., Frankenberg, C., Jiang, Z., & Blake, D. R. (2014). Mapping of North American methane emissions with high spatial resolution by inversion of SCIAMACHY satellite data. *Journal of Geophysical Research: Atmospheres, 119*(12), 7741-7756. https://agupubs.onlinelibrary.wiley.com/doi/abs/10.1002/2014JD021551

World Meteorological Organization, State of the Climate in Africa 2020, available at: https://storymaps.arcgis.com/stories/f7f88788f4c6463f96d228c07937310f, last access: Apr 18, 2022.

Zhang, G., Xiao, X., Dong, J., Xin, F., Zhang, Y., Qin, Y., et al. (2020). Fingerprint of rice paddies in spatial–temporal dynamics of atmospheric methane concentration in monsoon Asia. *Nature Communications, 11*(1), 554. https://doi.org/10.1038/s41467-019-14155-5

Zhang, Y., Jacob, D. J., Lu, X., Maasakkers, J. D., Scarpelli, T. R., Sheng, J. X., et al. (2021). Attribution of the accelerating increase in atmospheric methane during 2010–2018 by inverse analysis of GOSAT observations. *Atmos. Chem. Phys., 21*(5), 3643-3666. https://acp.copernicus.org/articles/21/3643/2021/